

## Origin of the Pinning of Drifting Monostable Patterns

M. G. Clerc,<sup>1</sup> C. Fernandez-Oto,<sup>1</sup> M. A. García-Ñustes,<sup>1</sup> and E. Louvergneaux<sup>2</sup>

<sup>1</sup>*Departamento de Física, Facultad de Ciencias Físicas y Matemáticas, Universidad de Chile, Casilla 487-3, Santiago, Chile*

<sup>2</sup>*Laboratoire de Physique des Lasers, Atomes et Molécules, UMR CNRS 8523, Université Lille 1, 59655 Villeneuve d'Ascq Cédex, France*

(Received 10 April 2012; revised manuscript received 29 June 2012; published 5 September 2012; corrected 11 September 2012)

Under drift forces, a monostable pattern propagates. However, examples of nonpropagative dynamics have been observed. We show that the origin of this pinning effect comes from the coupling between the slow scale of the envelope to the fast scale of the modulation of the underlying pattern. We evidence that this effect stems from spatial inhomogeneities in the system. Experiments and numerics on drifting pattern-forming systems subjected to inhomogeneous spatial pumping or boundary conditions confirm this origin of pinning dynamics.

DOI: [10.1103/PhysRevLett.109.104101](https://doi.org/10.1103/PhysRevLett.109.104101)

PACS numbers: 05.45.-a, 42.65.Sf, 47.54.-r

Pattern formation far from equilibrium occurs in all domains of sciences through the spontaneous symmetry breaking of a ground state [1]. Structures, generated at the first threshold of spatial instability, are generally stationary and can be either of (i) localized or of (ii) extended-periodic type. In some particular cases, such patterns continuously drift at their onset, for instance, when the system either possess (i) multiple coexisting states, (ii) a Hopf bifurcation or (iii) is subjected to cross advection or flow. In the first context, spatially localized interfaces connecting different states propagate due to the interplay between state energies. In the second one, a spontaneous parity breaking instability occurs that produces steadily drifting patterns [2,3]. In the third one, the induced cross convection forces the global patterns to drift [4,5]. However, in all situations, it has been observed that the structure could remain motionless or pinned [6–16].

In multistable systems, this phenomenon is called the “pinning effect” and was envisaged by Y. Pomeau more than 20 years ago [17,18]. This is the case for, e.g., in an homogeneous and a patterned state [19,20] or else two patterned states [21]. Pinning effect is a result of the competition between different energetic states that produces front propagation and spatial modulations that tend to block the motion by introducing periodic potential barriers in the dynamics of the front core [7,15]. Depending on the dominant effect, the front can stay motionless (locked) over a region of the parameter, called the pinning range. Above a critical value of the control parameter, the pinning-depinning transition occurs and the localized pattern (front or domain wall) propagates with periodic leaps. Increasing further the control parameter, the velocity of the interface becomes constant in space and time.

The same phenomenon is encountered in drifting monostable systems where single patterns are propagating [6,9,13,14]. In the latter, the pinning effect is also present. Theoretical works on pinning behavior have discussed the effects of the spontaneous translation symmetry breaking

for a second order transition system [22] or else “nonadiabaticity” for a first order transition system [7]. However, no general framework has been developed to elucidate the underlying locking mechanism in the class of monostable systems. Hence, a theoretical work is required for drifting monostable pattern systems that can be unified with the pinning theory developed in multistable systems.

In the present Letter, we show theoretically, numerically and experimentally that pinning-depinning transitions induced by spatial inhomogeneities in monostable systems come from the coupling between the small scale of the pattern modulation and the large scale of its amplitude envelope. This coupling, which is in contradiction with the standard multiple scale development assumption, appears as nonresonant terms in the amplitude equation. The analytical averaged phase velocity of the pattern agrees quite well with experimental dynamics of drifting patterns in a convective Kerr optical feedback system subject to a Gaussian transverse inhomogeneity.

In one-dimensional spatially extended convective systems, a well established pattern formed after a first instability threshold drifts as a consequence of a spatial asymmetric nonlocal interaction. A prototype model used to describe this effect is the drifting Swift-Hohenberg (SH) equation [23],

$$\partial_t u = \varepsilon u - u^3 - (\partial_{xx} + q^2)^2 u + \gamma \partial_x u + \delta u^2, \quad (1)$$

where  $u(x, t)$  is a scalar field,  $\varepsilon$  is the bifurcation parameter,  $q$  is the pattern wave number,  $\gamma$  accounts for drift source of the pattern and  $\delta$  is the nonlinear response coefficient. The SH model was introduced to describe the onset of Rayleigh-Benard convection; however, recent generalizations have been used intensively to account for pattern formation in several systems [23]. Equation (1) describes a supercritical bifurcation where the variable and parameters scale as  $u \sim \varepsilon^{1/2}$ ,  $q \sim \mathcal{O}(1)$ ,  $\partial_x \sim \varepsilon^{1/2}$ , and  $\partial_t \sim \varepsilon$  where  $\varepsilon \ll 1$ . For  $\varepsilon < 0$ , the system presents a stable uniform state  $u(x, t) = 0$ . At  $\varepsilon = 0$  the system bifurcates,

the uniform solution becomes unstable, giving rise to pattern formation. For  $\varepsilon > 0$ , the pattern amplitude, at wave number  $k_c = \pm q$ , grows as the square root of  $\varepsilon$ .

To reveal the pinning—depinning phenomenon in the SH model, we performed numerical simulations with two different boundary conditions: (i) Neumann ( $\partial_x u = 0$ ) and (ii) periodic. Figure 1 displays the pattern mean speed  $\langle v \rangle$  for different values of the drift parameter  $\gamma$ . Neumann boundary conditions (black dots) impose a strong spatial variation of the amplitude close to borders [Fig. 1(a)]. Remarkably, under these conditions, the system exhibits a pinning range. Within it, the drifting pattern is pushed to one side reaching a stationary state after a transient state. Figure 1(b) shows the final steady state for this case. Just above the pinning-depinning transition, the pattern moves with periodic leaps [Figs. 1(a) and 1(c)]. On the other hand, for periodic boundary conditions, the system displays a constant envelope over the whole space. The insets of Figs. 1(d) and 1(e) show this feature. For this case, the pattern drifts with nonzero velocity for any value of parameter  $\gamma \neq 0$  (dotted line in Fig. 1). The system moves with almost a constant speed.

It is important to note that spatial inhomogeneities of a parameter lead also to a pinning-depinning effect. Numerical simulations performed with a Gaussian

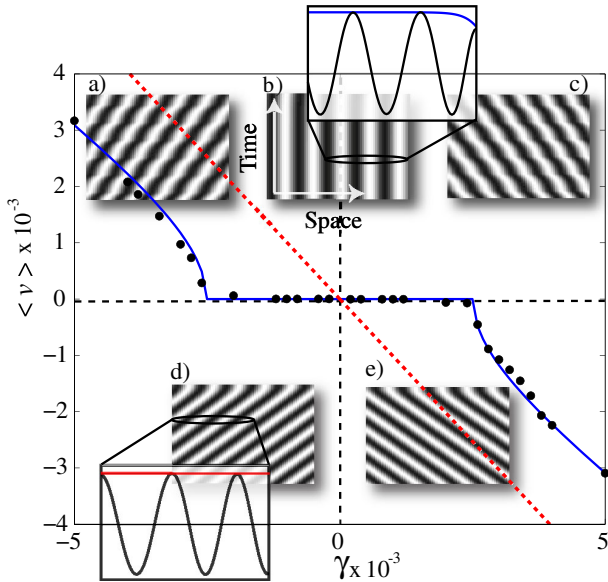


FIG. 1 (color online). Numerical pattern phase velocity  $\langle v \rangle$  versus drifting parameter  $\gamma$  (black dots) from Eq. (1). The blue solid line and red dashed line correspond to the velocity for Neumann boundary conditions [fitting obtain using Eq. (6)] and periodic conditions, respectively. Insets: Spatiotemporal pattern evolution is shown. A schematic image (zoom) of the pattern and the envelope close to the borders are also included (solid line). (a)–(c) Null flux boundary conditions and (d), (e) periodic boundary conditions. System parameters are  $\varepsilon = 0.09$ ,  $q = 0.5$ ,  $\delta = 1$  and (a)  $\gamma = -3.2 \times 10^{-3}$ , (b)  $\gamma = 2 \times 10^{-3}$ , (c)  $\gamma = 3.2 \times 10^{-3}$ , (d)  $\gamma = -1 \times 10^{-3}$ , (e)  $\gamma = 1 \times 10^{-3}$ .

variation of the parameter  $\varepsilon$ , i.e.,  $\varepsilon = \varepsilon_0 + a_0 e^{-(x-x_0)/2\sigma^2}$ , display a similar behavior to those observed for the Neumann boundary condition. Indeed, the Gaussian spatial dependence of  $\varepsilon$  imposes a smooth amplitude variation at the borders inducing a boundary conditionlike.

It is clear from these results that boundary conditions induce spatial variations for the pattern envelope even comparable to its modulation amplitude. As a consequence, the system displays a pattern envelope-modulation coupling close to borders leading to the pinning-depinning of the front as demonstrated in spatially modulated media [19–21].

To assess the above proposition, let us consider the amplitude equation approach of Eq. (1). Close to the bifurcation ( $\varepsilon \ll 1$ ), using the ansatz:  $u(x, t) = A(y \sim \mathcal{O}(\sqrt{\varepsilon}), t) \exp(ik_c x) / \sqrt{3 - 2\delta} + \text{c.c.}$  in Eq. (1) and imposing a solvability condition to calculate nonlinear corrections [23], we get

$$\partial_t A = \varepsilon A - |A|^2 A + i\beta A + \alpha \sqrt{\varepsilon} \partial_y A + \varepsilon \partial_{yy} A, \quad (2)$$

where  $\beta \equiv q\gamma$  stands for the phase velocity at  $q$ ,  $\alpha \equiv \gamma/2q$  accounts for the group velocity, and considering an appropriate spatial scaling. This conventional convective amplitude equation does not exhibit any phase velocity locking behavior [18]. Indeed, the amplitude equation approach is based on the separation of spatial evolution scales [24]. Such separation becomes relevant in the solvability condition which implies an inner product of the form,  $\langle f|g \rangle = (\sqrt{\varepsilon} k_c / 2\pi) \int_y^{y+2\sqrt{\varepsilon}\pi/k_c} f(y, x/\sqrt{\varepsilon}) g^*(y, x/\sqrt{\varepsilon}) dx$  where  $y$  refers to the slow scale (amplitude),  $x$  is the fast scale (patten), and  $\{f, g\}$  are periodic functions in  $x$ . Considering  $\sqrt{\varepsilon} \rightarrow 0$ , the spatial variation of the pattern envelope is slow enough with respect to the underlying pattern modulation wavelength ( $\partial_x A \ll k_c A / \sqrt{\varepsilon}$ ). In the case of Neumann boundary conditions, however, the coupling between the pattern envelope and its modulation close to the borders breaks the validity of this scale separation assumption which turns out to be no longer satisfied [18]. Following the asymptotic expansion of the Laplace integral [25], we obtain the corrective—nonresonant—terms to the amplitude equation [Eq. (2)] in the limit  $\sqrt{\varepsilon} \rightarrow 0$  [21,25]. The resulting amended amplitude equation then reads,

$$\begin{aligned} \partial_t A = & \varepsilon A - |A|^2 A + i\beta A + \alpha \sqrt{\varepsilon} \partial_y A + \varepsilon \partial_{yy} A \\ & - \frac{i\rho\sqrt{\varepsilon}}{3} \times [3\partial_y A^2 e^{ik_c y/\sqrt{\varepsilon}} \\ & - 3\partial_y |A|^2 e^{-ik_c y/\sqrt{\varepsilon}} - \partial_y \bar{A}^2 e^{-3ik_c y/\sqrt{\varepsilon}}], \end{aligned} \quad (3)$$

where  $\rho = \delta\pi/\sqrt{3-2\delta}q^2$ . Notice that nonresonant terms—the three last terms of Eq. (3)—become relevant when the spatial derivative of the envelope is no longer negligible, e.g., close to borders. This leads to a coupling between the envelope and the spatial modulation of the underlying pattern. These terms appear as soon as the system has finite transverse size (boundary conditions) or

possesses inhomogeneous parameters, which is quite often the case in reality.

To emphasize the effects of the corrective terms, we performed numerical simulations of Eq. (3). We considered two different boundary conditions: (i) Neumann condition,  $\partial_x A = 0$  and (ii) Dirichlet condition,  $A = 0$ . Measuring the time evolution of the spatially averaged phase  $d\langle\phi(x, t)\rangle_x/dt$ , where  $\langle\phi(x, t)\rangle_x \equiv 1/L \int_0^L \phi(x, t) dx$ , we get the averaged phase speed  $\langle v \rangle$  of the pattern. Figure 2, summarizes our numerical results for a system size of  $L = 600$ . For Neumann boundary conditions, the amplitude envelope is homogeneous in space. Then, non-resonant terms are equal to zero. The averaged phase speed  $\langle v \rangle$  increases linearly with the drift parameter  $\beta$  (Fig. 2, red dashed line). On the other hand, for Dirichlet conditions, we obtain large amplitude variations as  $A$  goes to zero at the borders, so that terms such as  $\partial_x A^2$  (i.e., nonresonant terms) play a prominent role. There exists a pinning region over a large interval of values of  $\beta$ . Figure 2(b) shows the spatiotemporal diagram of the reconstructed field  $u(x, t)$  from  $A(x, t)$ . It is clear that pattern remains stationary even for nonzero values of  $\beta$ . Above a critical value  $\beta_c$ , the pattern drifts with periodical leaps (Fig. 2(c)).

To analytically understand the above dynamical behavior, we derive an explicit expression for the pattern speed  $\langle v \rangle$  as a function of parameter  $\beta$ . Let us consider the polar representation  $A(x, t) = R(x, t)e^{i\phi(x, t)}$ , where  $R(x, t)$  and  $\phi(x, t)$  are the envelope modulus and phase, respectively. Replacing the polar representation in Eq. (3), and taking the imaginary part, we obtain,

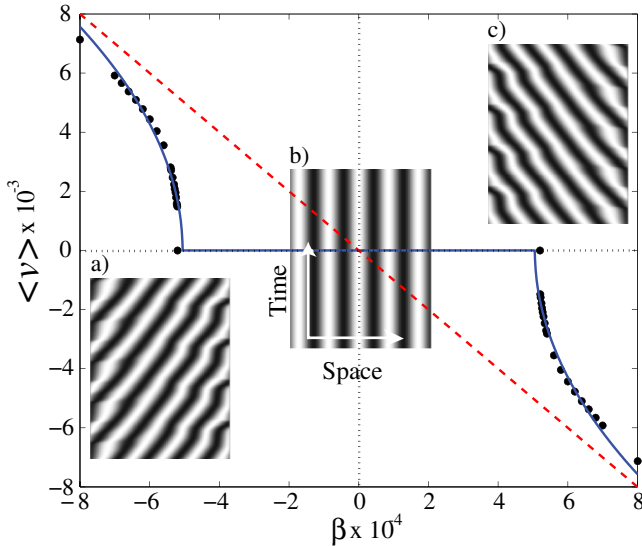


FIG. 2 (color online). Numerical computed pattern phase velocity  $\langle v \rangle$  versus drifting parameter  $\beta$  from Eq. (3) for Dirichlet (black dots) and periodic conditions (red dashed line). Curve fitting (blue solid line) with Eq. (6),  $\beta_c = 4.5 \times 10^{-4}$ . Insets: Spatiotemporal pattern evolution of a reconstructed field  $u(x, t)$  from  $A(x, t)$  with  $\varepsilon = 0.4$ ,  $\rho = 0.1$ ,  $L = 600$ , and (a)  $\beta = -7.0 \times 10^{-4}$ , (b)  $\beta = 3.0 \times 10^{-4}$ , and (c)  $\beta = 7.0 \times 10^{-4}$ .

$$\begin{aligned} R\partial_t\phi &= R\partial_{xx}\phi + 2R\partial_x\phi\partial_x R + \beta R + \alpha R\partial_x\phi \\ &+ 2\rho R\partial_x R \cos(k_c x + \phi) - 2\rho R^2\partial_x\phi \sin(k_c x + \phi) \\ &- 2\rho R\partial_x R \sin(k_c x). \end{aligned} \quad (4)$$

The real part determines the dynamics of  $R(x, t)$  which, at dominant order, is stationary and independent of  $\rho$ . As depicted in Fig. 3,  $\phi(x, t)$  is composed of two different superimposed temporal dynamic behaviors: (i) a periodic-like and (ii) a monotonically increasing one. Based on this observation, we propose the following ansatz:  $\phi(x, t) = \phi_\omega(x, t) + \psi(t)$  where  $\phi_\omega$  and  $\psi$ , respectively, account for the periodic (with dominant frequency  $\omega$ ) and the linear dynamics. Averaging Eq. (4) on space, we obtain a time dependent only expression. Next, let us take as the time average  $\langle\phi(x, t')\rangle_t \equiv \frac{\omega}{T} \int_t^{t+T} \phi(x, t') dt'$ . Denoting  $\langle\langle f(x, t) \rangle\rangle_t \equiv \langle f(x, t) \rangle_{x,t}$ , it is clear that the terms of the form  $\langle R\partial_x R F(\phi_\omega) \rangle_{x,t}$  where  $F(\phi_\omega)$  is a periodic function, are equal to zero from periodicity arguments. Meanwhile, terms of the form  $\langle R^2\partial_x\phi_\omega F(\phi_\omega) \rangle_{x,t}$  remain. Close to the pinning-depinning transition,  $d\langle\phi\rangle_x/dt$  has a slow dynamics. Therefore, the slope of  $\psi(t)$  remains invariant on time, i.e.,  $\psi(t) \equiv \langle\psi(t')\rangle_t$ . Subsequently, using trigonometric relations, Eq. (4) reads

$$\dot{\psi}(t) = \beta - 2\rho\sqrt{A_0^2 + B_0^2} \cos(\psi + \xi), \quad (5)$$

where  $A_0 = \langle R^2\partial_x\phi_\omega \sin(kx + \phi_\omega) \rangle_{x,t} / \langle R(x) \rangle_{x,t}$ ,  $B_0 = \langle R^2\partial_x\phi_\omega \cos(kx + \phi_\omega) \rangle_{x,t} / \langle R(x) \rangle_{x,t}$ , and  $\cos(\xi) = B_0 / \sqrt{A_0^2 + B_0^2}$ . Equation (5) can be interpreted as an overdamping particle under the influence of a periodical and constant force. Solving analytically Eq. (5) we get the following average speed [19]:

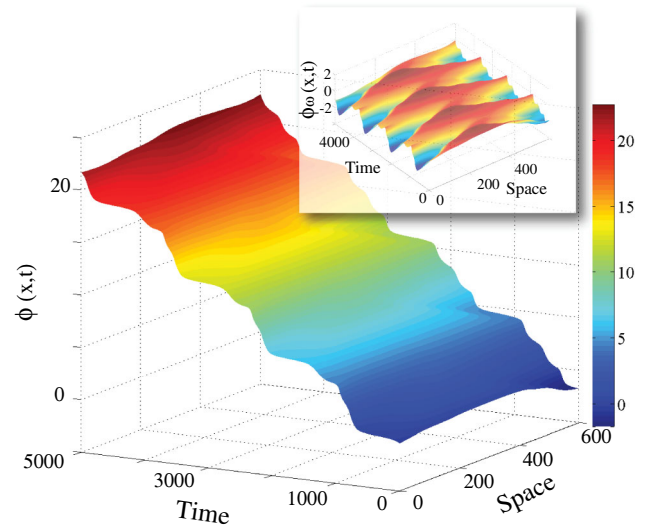


FIG. 3 (color online). Spatiotemporal diagram for  $\phi(x, t)$  with  $\varepsilon = 0.4$ ,  $\rho = 0.1$ ,  $k_c = 0.1$  and  $\beta = 7.0 \times 10^{-4}$ . Inset: Spatiotemporal diagram for  $\phi_\omega(x, t)$ .

$$\langle v \rangle = \sqrt{\beta^2 - \beta_c^2}, \quad (6)$$

where  $\beta_c \equiv |2\rho\sqrt{A_0^2 + B_0^2}|$  locates the pinning-depinning transition. Close to  $\beta_c$ , the system exhibits a saddle-node bifurcation with the pattern velocity increasing as the square root of  $\beta^2$ , whereas for larger values of  $\beta$ , it behaves as a linear function of  $\beta$ . Relation (6) has been derived initially in the context of front propagation in patterned systems [7]. Figure 2 shows the excellent fitting (blue solid line) of  $\langle v \rangle$  using Eq. (6) in the case of Dirichlet boundary conditions. Using the same fitting, we have a good agreement for the SH model with  $\beta_c = 2.6 \times 10^{-3}$  (see Fig. 1). Note that, from Eq. (5) it is also clear that if  $\rho$  is equal to zero, the nonresonant terms vanish. Therefore, the appearance of the pinning effect in the system is no longer observed, despite amplitude variations induced by the boundary conditions. Hence, the phase velocity is linearly proportional to  $\beta$ , in good agreement with Neumann conditions.

To provide an experimental verification of the pinning-depinning phenomenon in a drifting monostable pattern system, we consider the feedback optical system described in Refs. [26–28] which consists of a Kerr medium subjected to optical feedback provided by a mirror tilted by an angle  $\theta$  [see Fig. 4(a)]. It consists in a nematic liquid crystal (LC) layer irradiated by a laser beam (**F**) which is reflected back onto the sample (**B**) by a simple plane mirror placed at a variable distance  $d$  from the LC layer [Fig. 4(a)]. It is straightforward to derive a similar amended amplitude equation such as equation (3) from the model [29] which describes this experimental system. The full and lengthy expressions of these coefficients, as a function of the experiment parameters, will be reported elsewhere [30]. The nonlinear medium is a  $50 \mu\text{m}$  thick layer of  $E_7$  LC homeotropically anchored with response time  $\tau$  and diffusion length  $l_d$  which are equal to 2.3 s and  $10 \mu\text{m}$ , respectively, [31]. The beam is delivered by a monomode frequency doubled  $\text{Nd}^{3+} : \text{YVO}_4$  laser ( $\lambda_0 = 532 \text{ nm}$ ) which is shaped by means of two cylindrical telescopes in order to achieve a transverse quasi-monodimensional (1D) pumping (beam diameters  $\approx 93 \mu\text{m} \times 650 \mu\text{m}$ ). The optical feedback length  $d$  is equal to 5 mm. The reflected beam **B** is shifted transversely with respect to the incoming forward beam **F**. The translational shift  $h$  accounts for the distance between the two beams on the LC sample. For a typical feedback length  $d = 5 \text{ cm}$ , the angle  $\theta$  is of order of 4 mrad,  $h \approx 2l_d = 20 \mu\text{m}$  (to be compared with the pattern wavelength— $103 \mu\text{m}$ —in the conditions of a uniform pump profile). In the following,  $h$  will be given in units of  $l_d$  to keep the same units as for analytical predictions. The reflected beam is monitored after its second passage through the LC layer  $B_{\text{out}}$  (Fig. 4(a)). The pumping has a Gaussian shape, as a sort of Dirichlet boundary condition. Associated with the pattern drift induced by the translational shift  $h$ , the system

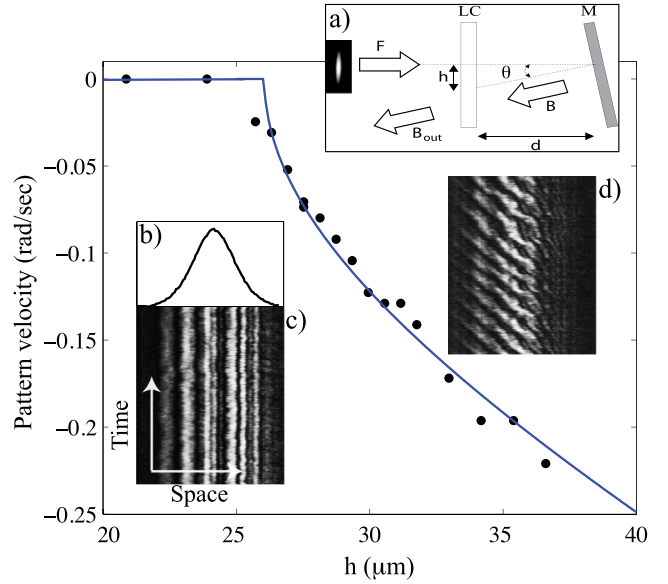


FIG. 4 (color online). Experimental phase velocity of a Kerr media subject to optical feedback (black dots) and its respectively theoretical fitting [Eq. (6)] (a) Experimental setup. Liquid crystal (LC) layer;  $M$  feedback mirror;  $F$  input optical field;  $B$  backward optical field;  $B_{\text{out}}$  output optical field sent to CCD cameras;  $\theta$  mirror tilt angle;  $d$  feedback length. (b) Laser intensity profile. Evolution of the experimental phase velocity versus the translational shift  $h$ . The considered parameters are  $d = 5 \text{ mm}$ ,  $I = 634 \text{ W/cm}^2$ , (c)  $h = 20.9 \mu\text{m}$  and (d)  $h = 27 \mu\text{m}$ . Spatiotemporal picture sizes (c), (d) are  $590 \mu\text{m} \times 800 \text{ s}$ .

presents all the ingredients for pinning-depinning transition. We then focus on the phase velocity evolution of the convective modes versus the lateral shift  $h$ .

As we can see in Fig 4, there is a good agreement between the predictions and the experimental observations on all the points. More specifically, the spatial dependence of the convective systems leads to the pinning phenomenon. The measured phase velocity evolves as  $\sqrt{h^2 - h_c^2}$  close to the pinning frontier  $h \approx 2.8l_d$ . This confirms the observations reported in [14]. In addition, Eq. (6) accurately describes the pinning-depinning transition. For this particular case, the spatial coupling between the pattern and the envelope variations is produced by the Gaussian profile of the pump beam (Fig. 4(b)). In fact, the coupling is present in almost all the space, given the small number of pattern wavelengths close to the maximum of the profile of the beam (aspect ratio  $\sim 6$ ). Figure 4(c) displays a spatiotemporal recording of the optical pattern profile exhibiting a pinned behavior. Above the pinning-depinning transition, we observe the expected pattern propagation with almost periodic leaps [Fig. 4(d)]. The aperiodicity comes from internal noise.

In conclusion, our work generalizes the pinning theory developed in multistable systems to all systems: Pinning phenomenon comes from the coupling between the slow

scale of the pattern envelope to the fast scale of its modulation.

The authors acknowledge financial support from Project No. ANR-2010-INTB-402-02 (ANR-CONICYT 39), “Colors.” M.G.C. and M.A.G-N. are thankful for the financial support of FONDECYT Projects No. 1120320 and No. 3110024, respectively. This research was supported in part by the Centre de la Recherche Scientifique (CNRS) and by the “Conseil Régional Nord—Pas de Calais,” “The Fonds Européen de développement Economique de régions.” C.F.O. acknowledges the financial support of CONICYT by Beca Magister Nacional and Program of Ayuda de Estadías Cortas de Investigación of University of Chile.

- 
- [1] G. Nicolis and I. Prigogine, *Self-Organization in Nonequilibrium Systems: From Dissipative Structures to Order through Fluctuations* (John Wiley & Sons, New York, 1977).
- [2] K. Jung, M. Lücke, and P. Büchel, *Phys. Rev. E* **54**, 1510 (1996).
- [3] E. Knobloch, J. Hettel, and G. Dangelmayr, *Phys. Rev. Lett.* **74**, 4839 (1995).
- [4] R. Briggs, *Electron-Stream Interaction with Plasmas* (MIT, Cambridge, MA, 1964).
- [5] P. Huerre and P. Monkewitz, *Annu. Rev. Fluid Mech.* **22**, 473 (1990).
- [6] I. Rehberg, E. Bodenschatz, B. Winkler, and F. Busse, *Phys. Rev. Lett.* **59**, 282 (1987).
- [7] D. Bensimon, B. Shraiman, and V. Croquette, *Phys. Rev. A* **38**, 5461 (1988).
- [8] B. Malomed, A. Nepomnyashchy, and M. Tribelsky, *Phys. Rev. A* **42**, 7244 (1990).
- [9] D. Ohlsen, S. Yamamoto, C. Surko, and P. Kolodner, *J. Stat. Phys.* **64**, 903 (1991).
- [10] C.M. Surko, D.R. Ohlsen, S.Y. Yamamoto, and P. Kolodner, *Phys. Rev. A* **43**, 7101 (1991).
- [11] O. Jensen, V. Pannbacker, G. Dewel, and P. Borckmans, *Phys. Lett. A* **179**, 91 (1993).
- [12] P. Kolodner, *Phys. Rev. E* **48**, R4187 (1993).
- [13] J. Seipenbusch, T. Ackemann, B. Schäpers, B. Berge, and W. Lange, *Phys. Rev. A* **56**, R4401 (1997).
- [14] T. Ackemann, B. Schapers, J.P. Seipenbusch, Y.A. Logvin, and W. Lange *Chaos Solitons Fractals* **10**, 665 (1999).
- [15] L. Pismen, *Springer Series in Synergetics* (Springer-Verlag, Berlin, 2006).
- [16] M. Schwartz and T. Solomon, *Phys. Rev. Lett.* **100**, 028302 (2008).
- [17] Y. Pomeau, in *Cellular Structures in Instabilities*, edited by J.E. Wesfreid and S. Zaleski, Lecture Notes in Physics Vol. 210 (Springer, Berlin, 1984).
- [18] Y. Pomeau, *Physica* (Amsterdam) **23D**, 3 (1986).
- [19] F. Haudin, R.G. Elías, R.G. Rojas, U. Bortolozzo, M.G. Clerc, and S. Residori, *Phys. Rev. E* **81**, 1 (2010).
- [20] M.G. Clerc, C. Falcon, D. Escaff, and E. Tirapegui, *Eur. Phys. J. Special Topics* **143**, 171 (2007).
- [21] U. Bortolozzo, M.G. Clerc, F. Haudin, R.G. Rojas, and S. Residori, *Adv. Nonlinear Opt.* **2009**, 1 (2009).
- [22] E. Knobloch, J. Hettel, and G. Dangelmayr, *Phys. Rev. Lett.* **74**, 4839 (1995).
- [23] M. Cross and P. Hohenberg, *Rev. Mod. Phys.* **65**, 851 (1993).
- [24] J. Kevorkian, *Multiple Scale and Singular Perturbation Methods, Applied Mathematical Sciences* (Springer-Verlag, Berlin, 1996), 1st ed., Vol. 114.
- [25] C.M. Bender and S.A. Orzag, *Advanced Mathematical Methods for Scientists and Engineers* (McGraw-Hill, New York, 1978), 1st ed.
- [26] E. Louvergneaux, *Phys. Rev. Lett.* **87**, 244501 (2001).
- [27] E. Louvergneaux, C. Szwaj, G. Agez, P. Glorieux, and M. Taki, *Phys. Rev. Lett.* **92**, 043901 (2004).
- [28] G. Agez, P. Glorieux, M. Taki, and E. Louvergneaux, *Phys. Rev. A* **74**, 043814 (2006).
- [29] G. Dalessandro and W.J. Firth, *Phys. Rev. A* **46**, 537 (1992).
- [30] M.G. Clerc, C. Fernandez-Oto, M.A. García-Ñustes, and E. Louvergneaux (to be published).
- [31] G. Agez, P. Glorieux, C. Szwaj, and E. Louvergneaux, *Opt. Commun.* **245**, 243 (2005).